Frequency-domain quantum computation to selectively manipulate many qubits

Satoshi Nakamura,* Hayato Goto, Mamiko Kujiraoka, and Kouichi Ichimura
Toshiba Corporation Research and Development Center, Saiwai-ku, Kawasaki 212-8582, Japan
(Received 26 December 2013; revised manuscript received 9 December 2014; published 9 January 2015)

We propose an implementation scheme of a frequency-domain quantum computation (FDQC) to avoid major gate errors accompanying the computation. The FDQC is a way to implement many solid-state qubits defined in a frequency domain without distinction of their positions. The FDQC has some gate errors due to unwanted effects of operation lights on qubits. We investigate conditions to perform gates suppressing the errors using a model of the FDQC with the unwanted interactions. Consequently, we find a scheme to selectively manipulate many qubits using the FDQC.

DOI: 10.1103/PhysRevA.91.012309 PACS number(s): 03.67.Lx, 32.80.Qk

I. INTRODUCTION

Various physical implementations of the quantum computation have been studied [1]. A promising physical implementation of the computation is that of using adiabatic passages [2–4]. Quantum gates can be robustly performed with adiabatic passages using the dark state [5]. The adiabatic passages for quantum gates have been demonstrated in some systems: Rydberg atoms [6], an ion trap [7], rare-earth-ion-doped crystals [8,9], and nitrogen-vacancy centers in diamond [10].

There are some systems in which we can hardly identify positions of qubits in the above systems. Quantum gates based on adiabatic passages using qubits identified by their frequencies have been proposed to employ such systems for quantum computations [11]. In the proposal, states of individual ions in solids are employed as qubits, the ions are identified by their transition frequencies, and these gates are performed using operation lights which are resonant with each transition. If inhomogeneous broadening of the transitions is larger than homogeneous broadening, then these gates are feasible. A frequency-domain quantum computation (FDQC) based on such gates enables us to manipulate many solid-state qubits selectively without identification of the positions of the qubits.

In the FDQC, operation lights with detuning interact with transitions which are not intended to operate because qubits are irradiated regardless of their positions. This unwanted interaction causes gate errors of the FDQC. If frequency differences of the transitions are large enough, the gate errors are suppressed. However, when we would like to implement many qubits in a finite-frequency range, the frequency differences cannot be sufficiently large. Therefore, it is desirable to suppress the gate errors even if the frequency differences are small.

The purpose of this paper is to investigate the conditions to suppress gate errors due to unwanted interactions in the FDQC. In particular, we focus on errors of the two-qubit gate which are expected to have a nontrivial property. The two-qubit gate using adiabatic passage is based on a cavity mediated adiabatic passage (CMAP) using qubits coupled to a cavity mode [12]. Therefore, we introduce the unwanted interactions to the model of the CMAP, and investigate conditions to perform the CMAP for high fidelity in the model. In the investigation, the unwanted interactions are treated as the perturbation potential, and we evaluate the probabilities of nonadiabatic transitions during the manipulation of the CMAP by the perturbation theory. We analytically evaluate resonance conditions to increase the errors generated by nonadiabatic transitions. We numerically calculate the fidelity of the CMAP in a three-qubit system around the resonance condition.

II. MODEL

The CMAP is a technique to manipulate quantum states of multilevel systems in a cavity by coherent lasers.

Figure 1(a) shows a multiqubit system as an example of a system for the CMAP in a FDQC. Each four-level system X_i has states $|0\rangle_i$, $|1\rangle_i$, $|2\rangle_i$, and $|e\rangle_i$. The states $|0\rangle_i$ and $|1\rangle_i$ represent a qubit, and the state $|2\rangle_i$ is an ancilla state. We use X_i's which have $|2\rangle_i - |e\rangle_i$ transitions coupled to the cavity mode with a coupling constant g. We assume that transitions between lower states of X_i have inhomogeneous broadening. Therefore, although all the $|2\rangle_i - |e\rangle_i$ transitions have the same frequency, $|1\rangle_i - |e\rangle_i$ transitions have various frequencies. Operation lights L_1 and L_2 are resonant with the $|1\rangle_1 - |e\rangle_1$ transition and $|1\rangle_2 - |e\rangle_2$ transition, respectively. We assume that the Rabi frequencies of interactions between L_1 and all the $|1\rangle_i - |e\rangle_i$ transitions are a common Ω_1 [13]. We assume also that the Rabi frequencies due to L_2 are a common Ω_2. γ is an energy-relaxation rate at excited states $|e\rangle_i$ and κ is a cavity-relaxation rate.

For the CMAP, we use Gaussian pulses described by

$$\Omega_1(t) = \Omega_0 \exp[-(t-\tau_1)^2/2\sigma^2]$$
$$\Omega_2(t) = \Omega_0 \exp[-(t-\tau_2)^2/2\sigma^2]. \quad (1)$$

Ω_0 is the peak value of $\Omega_{1,2}$, and σ is the width of $\Omega_{1,2}$. $\tau_{1,2}$ are times when $\Omega_{1,2}$ reach their peaks, respectively. $|n_1 n_2 n_3 \cdots n_N n_c\rangle$ denotes a state of N-qubit system in which states of X_i $(i = 1,2,\ldots,N)$ are $|n_i\rangle_i$ and the cavity mode has photon number n_c. The CMAP using Gaussian pulses [Eq. (1)] under $\tau_2 < \tau_1$ without unwanted interactions can transfer a state from an initial state $|12n_3 \cdots n_N 0\rangle$ to a final state $|21n_3 \cdots n_N 0\rangle$ $(n_3,\ldots,n_N = 0,1)$ [12].

However, there are some unwanted interactions during the CMAP operation in the FDQC. Interactions between L_1 and $|1\rangle_i - |e\rangle_i$ transitions $(i = 2,3,\ldots,N)$ and interactions between L_2 and $|1\rangle_i - |e\rangle_i$ transitions $(i = 1,3,4,\ldots,N)$ are unwanted. When L_1 and L_2 are resonant with the $|1\rangle_1 - |e\rangle_1$

*Corresponding author: satoshi20.nakamura@toshiba.co.jp

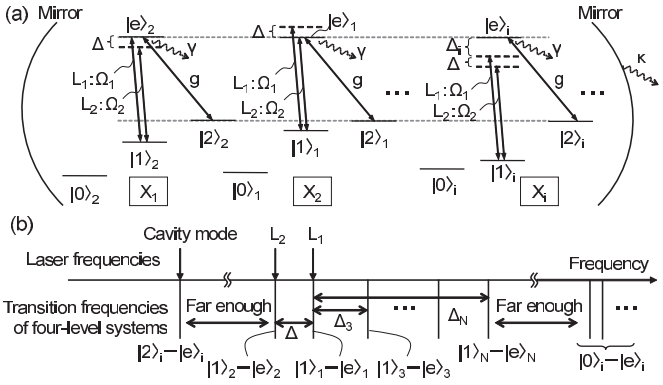

FIG. 1. (a) A model of qubits in a cavity for a CMAP in a FDQC. Each four-level system X_i has states $|0\rangle_i$, $|1\rangle_i$, $|2\rangle_i$, and $|e\rangle_i$. All of the $|2\rangle_i - |e\rangle_i$ transitions are coupled to the cavity mode with a coupling constant g. An operation light L_1 is resonant with the $|1\rangle_1 - |e\rangle_1$ transition, and L_2 is resonant with the $|1\rangle_2 - |e\rangle_2$ transition. $\Omega_{1,2}$ are Rabi frequencies due to $L_{1,2}$, respectively. Δ is the detuning between L_1 and the $|1\rangle_2 - |e\rangle_2$ transition, Δ_i are the detunings between L_1 and the $|1\rangle_i - |e\rangle_i$ transitions, γ is an energy-relaxation rate at states $|e\rangle_i$, and κ is a cavity-relaxation rate. (b) Schematic diagram of relations between transitions and lights in (a).

and $|1\rangle_2 - |e\rangle_2$ transitions, respectively, unwanted interactions are characterized by detunings Δ and Δ_j ($j \geqslant 3$), where Δ is defined as a frequency difference between the $|1\rangle_1 - |e\rangle_1$ transition and the $|1\rangle_2 - |e\rangle_2$ transition, and Δ_j are defined as frequency differences between the $|1\rangle_1 - |e\rangle_1$ transition and the $|1\rangle_j - |e\rangle_j$ transitions. There are $N-1$ detuning parameters in the N-qubit system. We assume that frequencies of the $|0\rangle_i - |1\rangle_i$ and $|1\rangle_i - |2\rangle_i$ transitions of each X_i are large enough to neglect the effects of $L_{1,2}$ to $|0\rangle_i - |e\rangle_i$ and $|2\rangle_i - |e\rangle_i$ transitions. Figure 1(b) shows the above relations between transitions and lights.

In the rotating-wave approximation, we take an interaction picture Hamiltonian H described by

$$
\begin{aligned}
&H(t) = H_1(t) + V(t) + D,\\
&\begin{cases}
H_1(t)/\hbar = \displaystyle\sum_{i=1}^{N} g a \sigma_{e2}^{(i)} + \Omega_1(t)\sigma_{e1}^{(1)} + \Omega_2(t)\sigma_{e1}^{(2)} + \text{H.c.},\\
V(t)/\hbar = \Omega_1(t)\left\{ e^{-i\Delta t}\sigma_{e1}^{(2)} + \displaystyle\sum_{j=3}^{N} e^{i\Delta_j t}\sigma_{e1}^{(j)} \right\}\\
\quad + \Omega_2(t)\left\{ e^{i\Delta t}\sigma_{e1}^{(1)} + \displaystyle\sum_{j=3}^{N} e^{i(\Delta+\Delta_j)t}\sigma_{e1}^{(j)} \right\} + \text{H.c.},\\
D/\hbar = -i\gamma \displaystyle\sum_{i=1}^{N} \sigma_{ee}^{(i)} - i\kappa a^\dagger a,
\end{cases}
\end{aligned}
\tag{2}
$$

which is suitable to investigate the gate errors. See Appendix A for a derivation. H is divided into the necessary interactions H_1, the unwanted interactions V, and relaxations D. H has oscillation terms in V. $\sigma_{ab}^{(i)}$ is an operator which transfers the state of X_i from $|b\rangle_i$ to $|a\rangle_i$. a and $a^\dagger$ are annihilation and creation operators of the cavity mode, respectively. We investigate conditions to perform the CMAP in high fidelity using H.

III. RESONANCE CONDITION

We assume the strong-coupling limit $\gamma = \kappa = 0$ to evaluate the gate error due to unwanted interactions in the CMAP. The initial state $|\psi(0)\rangle$ is fixed to the dark state $|\psi_0\rangle$, which is one of the eigenstates $|\psi_n\rangle$ of H_1. In the case of $\Omega_{1,2} \ll g$ [14], the state $|\psi(t)\rangle$ is given by $|\psi(t)\rangle = |\psi_0\rangle + \sum_n C_n^{(1)}(t)|\psi_n\rangle + \sum_n C_n^{(2)}(t)|\psi_n\rangle + O(V^3)(n \neq 0)$ in the perturbation theory of V. The coefficients $C_n^{(1,2)}$, which relate error probabilities, are described by

$$
\begin{aligned}
C_n^{(1)}(t) &= \frac{1}{i\hbar}\int_0^t dt' e^{-(E_n-E_0)t'/i\hbar}\langle\psi_n|V(t')|\psi_0\rangle,\\
C_n^{(2)}(t) &= \left(\frac{1}{i\hbar}\right)^2 \int_0^t dt' \int_0^{t'} dt'' e^{-(E_n-E_k)t'/i\hbar} e^{-(E_k-E_0)t''/i\hbar}\\
&\quad \times \langle\psi_n|V(t')|\psi_k\rangle\langle\psi_k|V(t'')|\psi_0\rangle.
\end{aligned}
\tag{3}
$$

E_n are the eigenvalues of $|\psi_n\rangle$. The time variations of E_n are smaller than the absolute values of E_n in the case of $\Omega_{1,2} \ll g$, since the variations of E_n depend on only the time variations of $\Omega_{1,2}$. In that case, integrals in Eq. (3) are integrable, and $C_n^{(1,2)}$ are inversely proportional to the exponents of the exponential functions in $C_n^{(1,2)}$. When the exponents are zero, the error probabilities diverge, so that the perturbation theory is unavailable. Considering oscillation terms in $V(t')$, we obtain resonance conditions using Δ and Δ_j ($j = 3,4,\ldots,N$),

$$
(E_n - E_0)/\hbar = \pm\Delta, \pm\Delta_j, \pm(\Delta + \Delta_j), \tag{4}
$$

$$
\begin{aligned}
&(E_k - E_0)/\hbar = \pm\Delta, \pm\Delta_j, \pm(\Delta + \Delta_j)\\
&(E_n - E_k)/\hbar = \pm\Delta, \pm\Delta_j, \pm(\Delta + \Delta_j).
\end{aligned}
\tag{5}
$$

When the conditions described by Eqs. (4) and (5) are satisfied, the errors of the CMAP are increased owing to increases of $C_n^{(1)}$ and $C_n^{(2)}$, respectively.

In the case of $\Omega_{1,2} \ll g$, the terms of $\Omega_{1,2}$ are negligible in H_1, and E_n are evaluated by the analogy of the vacuum Rabi splitting. The number of X_i which have population in two levels $|2\rangle_i$ and $|e\rangle_i$ is denoted by N_2, the eigenvalues of $(\sum_i \sigma_{e1}^{(i)})^2 + (\sum_i \sigma_{1e}^{(i)})^2 + (\sum_i \sigma_{ee}^{(i)})^2$ are denoted by $s(s+1)$, and the eigenvalues of $\sum_i \sigma_{ee}^{(i)}$ are denoted by $n_e/2 - s$. E_n are classified according to the total number of excitations $N_e = n_e + n_c$ and s [15,16]. Some of E_n are described by

$$
E_n/\hbar = \begin{cases}
\pm\sqrt{N_2}g & (N_e = 1, s = N_2/2)\\
0, \pm\sqrt{4N_2 - 2}g & (N_e = 2, s = N_2/2)\\
\pm\sqrt{N_2 - 2}g & (N_e = 2, s = N_2/2 - 1)
\end{cases}. \tag{6}
$$

See Appendix B for a derivation. $E_n/\hbar$ of the case of $(N_e = 1, s = N_2/2)$ is corresponding to the peak frequencies of the vacuum Rabi splitting. The resonance conditions represented by Eqs. (4) and (5) are analytically evaluated using Eq. (6) and $E_0 = 0$. To perform the high-fidelity CMAP in the FDQC, systems and operation lights have to avoid the resonance conditions.

IV. NUMERICAL SIMULATION

We numerically calculate the fidelity of a CMAP using a three-qubit system to investigate the behavior of errors via unwanted interactions around the resonance conditions. When the relaxation rates γ and κ are zero, the time evolution of states is calculated using time-dependent Schrödinger equations $i\hbar\frac{d}{dt}|\psi(t)\rangle = H(t)|\psi(t)\rangle$. When the system has relaxations, the time evolution of states is calculated using the Monte Carlo simulation based on the quantum jump approach [17]. In our calculation, the initial state is fixed to a state $|1210\rangle$, the state is evolved from $t = 0$ to $t = 10\sigma$ under Eq. (1), and the fidelity of the CMAP is defined as the probability of a state $|2110\rangle$ in the final state. The probability of the other states in the final state is the gate error. σ is fixed to $20/\Omega_0$ to suppress nonadiabatic effects. $\tau_{1,2}$ are optimized with respect to Ω_0.

Figure 2 shows detuning dependences of the errors of the CMAP. Figures 2(a) and 2(b) shows Δ dependence with $\Delta_3 = 10g$ and Δ_3 dependence with $\Delta = 10g$, respectively. Figures 2(c) and 2(d) show contour diagrams of the error in the Δ_3–Δ planes with $\Omega_0 = 0.05g$ and $\Omega_0 = 0.2g$, respectively. In these calculations, we assume that all relaxation rates are zero.

In Fig. 2, the errors increase in particular regions. In Fig. 2(a), the errors of $X_{1,2}$, which are probabilities of the states $|1210\rangle$, $|2e10\rangle$, $|2211\rangle$, and $|e210\rangle$ in the final state, increase around $\Delta = 0, \sqrt{2}g$. In Fig. 2(b), the errors of X_3, which are probabilities that the state of X_3 becomes states except $|1\rangle_3$ in the final state, increase around $\Delta_3 = 0, g, \sqrt{2}g, \sqrt{10}g$, and the errors of $X_{1,2}$ increase around $\Delta_3 = g, \sqrt{2}g$. There are the 19 regions in which the errors increase in Figs. 2(c) and 2(d). The regions in Fig. 2(c) are represented by the equations in Table I. All of the 19 regions are explained by analytic solution of second-order perturbation theory (see Appendix C).

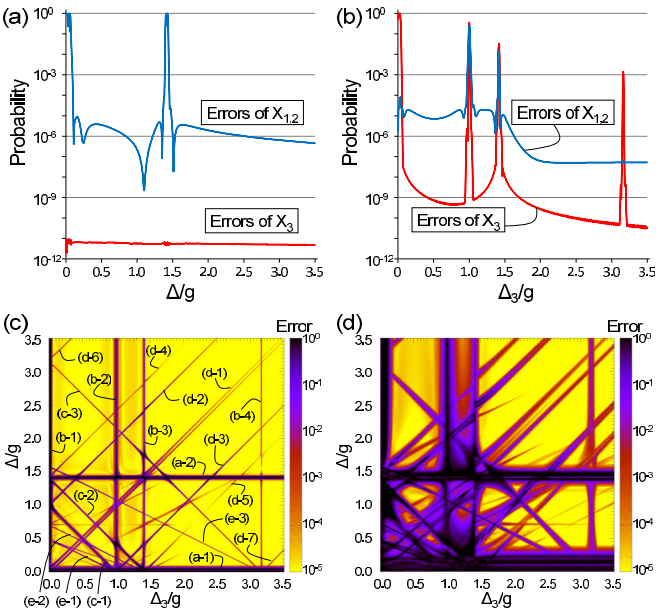

FIG. 2. (Color online) (a) Δ dependence of the errors. The error probability of the CMAP with $\Omega_0 = 0.05g$, $\tau_1 = 6.01\sigma$, $\tau_2 = 3.99\sigma$, and $\Delta_3 = 10g$ is plotted. Errors of $X_{1,2}$ represent a probability of the states $|1210\rangle$, $|2e10\rangle$, $|2211\rangle$, and $|e210\rangle$ in the final state, and errors of X_3 represent a probability that the state of X_3 becomes states except $|1\rangle_3$ in the final state. (b) Δ_3 dependence of the errors. The probabilities are plotted with $\Delta = 10g$. The other conditions are the same as those for (a). (c) Contour diagram of the error with $\Omega_0 = 0.05g$, $\tau_1 = 6.01\sigma$, and $\tau_2 = 3.99\sigma$. The contour diagram shows the error in the Δ_3–Δ plane. (d) Contour diagram of the error with $\Omega_0 = 0.2g$, $\tau_1 = 6.03\sigma$, and $\tau_2 = 3.97\sigma$.

TABLE I. Equations corresponding to the labels in Fig. 2(c).

(a − 1,2)	$\Delta = 0, \sqrt{2}g$
(b − 1,2,3,4)	$\Delta_3 = 0, g, \sqrt{2}g, \sqrt{10}g$
(c − 1,2,3)	$\Delta + \Delta_3 = g, \sqrt{2}g, \sqrt{10}g$
(d − 1,2,3,4,5,6,7)	$\Delta - \Delta_3 = 0, \pm g, \pm\sqrt{2}g, \pm\sqrt{10}g$
(e − 1,2,3)	$2\Delta + \Delta_3 = g, \sqrt{2}g, \sqrt{10}g$

The CMAP shows low error in $\Delta, \Delta_j \gg g$. In Figs. 2(c) and 2(d), there are also low-error regions avoiding the resonance conditions in $\Delta, \Delta_j < g$. In particular, there are large regions of low error in Fig. 2(c), in which Ω_0 is small and the gate time is long.

Actual systems have other error sources such as the energy relaxation or the cavity relaxation. In the above, the relaxations are neglected. We investigate the resonance conditions of unwanted interactions with the relaxations as follows. Figure 3 shows the Δ_3 dependences of the error of the CMAP with $\Delta = 10g$ for various relaxation rates.

Although there are the relaxations in the system, the peaks of errors are still around the resonance conditions, in particular, the errors suppressed even in $\Delta_3 < g$ regions by avoiding the resonance conditions.

V. DISCUSSION

We investigated the CMAP including the unwanted interactions. Although there are the unwanted interactions, the CMAP shows high fidelity by avoiding the resonance conditions. The high-fidelity regions in $\Delta, \Delta_j \gg g$ are trivial regions because the unwanted interactions become small as frequency differences of transitions become large. The high-fidelity regions in $\Delta, \Delta_j < g$ are nontrivial and useful regions to implement many qubits in a finite-frequency range.

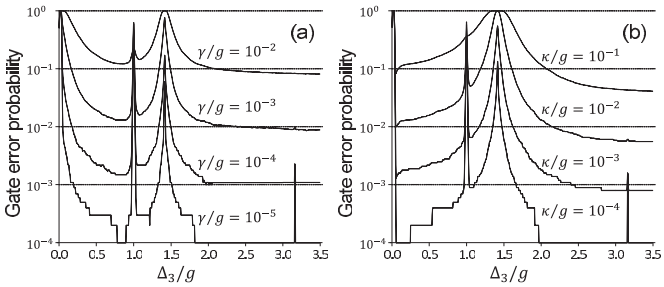

FIG. 3. (a) Δ_3 dependence of the error for various γ with $\Omega_0 = 0.05g$, $\tau_1 = 6.01\sigma$, $\tau_2 = 3.99\sigma$, $\Delta = 10g$, and $\kappa = 0$. The calculations are based on 10^4 times Monte Carlo simulation. (b) Δ_3 dependence of the error for various κ with $\gamma = 0$. The other conditions are the same as those for (a).

A strong-coupling system, which satisfies the condition of $\gamma,\kappa \ll g$, is required to reduce gate errors well in these high-fidelity regions. The system should have the long-coherence time, since the gate time should be long to suppress the nonadiabatic effects. However, the strong-coupling system with long-coherence time has not been realized. We discuss directions of development to realize the FDQC using two actual systems which have long-coherence times.

The first system is a rare-earth-ion-doped crystal Pr^{3+}:Y_2SiO_5 (Pr:YSO), which has long-coherence time and is a promising system for quantum information devices [18–21]. In the Pr:YSO, the inhomogeneous broadening between a pair of hyperfine sublevels of the lower states of the ${}^3H_4$–${}^1D_2$ transitions is 70 kHz, and the homogeneous broadening between ${}^3H_4$–${}^1D_2$ is several kHz [22]. Therefore, many qubits can be implemented using the transitions. However, the high-fidelity quantum gates cannot be performed even in any frequency regions avoiding the resonance condition, since actual relaxation parameters κ/g and γ/g are large. In our previous experimental study, $\kappa/2\pi$ of a sample is 1.3 MHz [23], and $g/2\pi$ of another sample is 15 kHz [24]. The energy-relaxation rate $\gamma/2\pi$ is about 1 kHz [25]. A cavity with lower loss and smaller mode volume is required to realize the FDQC using the Pr:YSO. If a Pr:YSO system with a cavity of 10^{-6} loss per round trip and the mode waist of wavelength scale is developed, then the parameters become $\kappa/2\pi \sim 1$ kHz [26] and $g/2\pi \sim 1$ MHz [27] ($\kappa/g \sim \gamma/g \sim 0.001$), and the gate errors are reduced to less than 10^{-2} even in the $\Delta < g$.

The second system is nitrogen-vacancy centers in a diamond (NV centers). NV centers have long-coherence time at room temperature, and are also promising systems of the quantum information devices [28]. A system of NV centers coupled to a photonic crystal cavity with $g/2\pi = 2.25$ GHz, $\gamma/2\pi = 0.013$ GHz, and $\kappa/2\pi = 0.16$ GHz ($\kappa/g \sim 0.07$, $\gamma/g \sim 0.006$) has been reported [29]. Improvement of g and κ is required to reduce gate errors to 10^{-2} in the $\Delta,\Delta_j < g$ region. There are high-fidelity regions in the $\Delta_3 > g$ region of Fig. 3 even for the above parameters. However, it is difficult to implement the FDQC in the systems because the homogeneous broadening of optical transitions of NV centers is larger than the inhomogeneous broadening of the spin levels. For example, the homogeneous broadening is about 50 MHz, and the inhomogeneous broadening is 5 MHz in Ref. [30]. The inhomogeneous broadening can be increased by an increase of the density of the NV centers, but the coherence time will be decreased. A different method to increase the inhomogeneous broadening is required to realize the FDQC using the NV centers. The inhomogeneous broadening is increased by the magnetic-field gradient because the resonance frequency of each NV center is split by the magnetic field [31]. If we apply the magnetic-field gradient of 50 mT per 1 μm, inhomogeneous broadening within 1 μm will be increased to over 1 GHz, which is larger than homogeneous broadening. Here, 1 μm is a typical size of the mode waist where NV centers coupled to a cavity are distributed, when the waist is reduced to the order of the wavelength of the mode.

The conditions for the high-fidelity FDQC obtained by our investigation will be useful when the FDQC is realized by the above development.

We showed numerical analyses only on a three-qubit system. The scheme to find the high-fidelity region can also be applied to the case of many-qubit systems. A candidate of high-fidelity regions can be found in regions avoiding the resonance conditions [Eqs. (4) and (5)] which are obtained analytically even in the many-qubit systems.

VI. SUMMARY

We investigated the major gate errors of the FDQC using adiabatic passage. The gate errors are generated by unwanted interactions because qubits are irradiated regardless of their positions. We analytically found out the resonance conditions in which the gate errors increase. We showed that high-fidelity gates are practicable, avoiding the resonance conditions even in $\Delta,\Delta_j < g$. This means that we obtained a useful implementation scheme which enables many qubits to be selectively manipulated in the FDQC.

APPENDIX A: THE INTERACTION PICTURE HAMILTONIAN

We explain the interaction picture Hamiltonian [Eq. (2)] of the cavity mediated adiabatic passage (CMAP). The model of the CMAP is described in Fig. 1. In Fig. 1(a), each four-level system X_i has states $|0\rangle_i$, $|1\rangle_i$, $|2\rangle_i$, and $|e\rangle_i$, and the energies of states $|j\rangle_i$ are $\hbar\omega_j^{(i)}$. The cavity mode and the operation lights $L_{1,2}$ have frequencies f_c and $f_{1,2}$, respectively.

The Schrödinger picture Hamiltonian of the CMAP including unwanted interactions in the rotating-wave approximation is described by

$$\begin{aligned} H_S(t)/\hbar = &\sum_{k=1}^{N}\left[\sum_{j=0,1,2,e}\omega_j^{(k)}\sigma_{jj}^{(k)} - i\gamma\sigma_{ee}^{(k)}\right] \\ &+ [2\pi f_c a^\dagger a - i\kappa a^\dagger a] \\ &+ \sum_{k=1}^{N}\left[ga\sigma_{e2}^{(k)} + \Omega_1(t)e^{-i2\pi f_1 t}\sigma_{e1}^{(k)}\right. \\ &\left. + \Omega_2(t)e^{-i2\pi f_2 t}\sigma_{e1}^{(k)} + \text{H.c.}\right]. \end{aligned} \tag{A1}$$

$\sigma_{ab}^{(k)}$ is an operator which transfers the state of X_k from $|b\rangle_k$ to $|a\rangle_k$. a and $a^\dagger$ are annihilation and creation operators of the cavity mode, respectively. Each term of the Hamiltonian represents the energy or interaction described below. The first term represents the energy of states and the energy relaxation of X_k. The second term represents the energy of the cavity mode and the cavity relaxation. The third term represents interactions between the cavity mode and $|2\rangle_k - |e\rangle_k$ transitions, between L_1 and $|1\rangle_k - |e\rangle_k$ transitions, and between L_2 and $|1\rangle_k - |e\rangle_k$ transitions.

There are various representations of the interaction picture Hamiltonian, which is $e^{iH_0t/\hbar}(H_S - H_0)e^{-iH_0t/\hbar}$, according to H_0. When two lasers interact with a transition, we cannot take a standard picture in which the interaction picture Hamiltonian has the energy terms including detuning parameters and does not have the oscillation terms. When the Hamiltonian has energy terms and oscillation terms, it is difficult to evaluate the probabilities of nonadiabatic transitions by the perturbation theory. Therefore, we take a representation in which the

interaction picture Hamiltonian has oscillation terms including detuning parameters and does not have energy terms. H_0 is defined by

$$H_0/\hbar \equiv \sum_{k=1}^{N}\left[\sum_{j=0,1,2,e}\left(\omega_j^{(k)}\sigma_{jj}^{(k)}\right)\right] + 2\pi f_c a^\dagger a \tag{A2}$$

to take such representation. The interaction picture Hamiltonian H described by Eq. (2) is obtained by this H_0 and the following relations:

$$\omega_e^{(1)} - \omega_1^{(1)} = 2\pi f_1, \tag{A3}$$

$$\omega_e^{(1)} - \omega_1^{(1)} = 2\pi f_2 + \Delta, \tag{A4}$$

$$\omega_e^{(2)} - \omega_1^{(2)} = 2\pi f_1 - \Delta, \tag{A5}$$

$$\omega_e^{(2)} - \omega_1^{(2)} = 2\pi f_2, \tag{A6}$$

$$\omega_e^{(j)} - \omega_1^{(j)} = 2\pi f_1 + \Delta_j, \tag{A7}$$

$$\omega_e^{(j)} - \omega_1^{(j)} = 2\pi f_2 + \Delta + \Delta_j, \tag{A8}$$

$$\omega_e^{(k)} - \omega_2^{(k)} = 2\pi f_c, \tag{A9}$$

for $(k = 1,2,\ldots,N)$ and $(j = 3,4,\ldots,N)$.

H does not have energy terms and there are detuning parameters only in the oscillation terms. The oscillation terms result from the unwanted interactions for the CMAP. We can analytically evaluate the probabilities of nonadiabatic transitions using this representation. In Sec. III, we analytically evaluate the resonance conditions by perturbation theory using H.

APPENDIX B: THE EIGENVALUES OF THE HAMILTONIAN

Equations (6), which are the eigenvalues of H_1 in Eq. (2), are derived as follows. This derivation is based on Refs. [16] and [17].

In the case of $\Omega_{1,2} \ll g$, H_1 is described by

$$H_1/\hbar = \sum_{i=1}^{N_2}\left(ga\sigma_{e2}^{(i)} + ga^\dagger\sigma_{2e}^{(i)}\right). \tag{B1}$$

H_1 operates in the two-state systems $|2\rangle_i - |e\rangle_i$ $(i = 1,2,\ldots,N_2)$, where N_2 denotes the number of X_i's which have population in the $|2\rangle$ or $|e\rangle$ during the CMAP. The number of X_i's whose states are $|e\rangle_i$ is n_e, and the photon number of the cavity mode is n_c. The total number of excitations is $N_e = n_e + n_c$. N_2 depends on N, N_e, and the initial state of the CMAP. For example, when the initial state is $|1210\rangle$ in the three-qubit system, N_2 is 2 for $N_e = 1$, and N_2 is 3 for $N_e = 2$. The eigenvalues of $(\sum_i \sigma_{e1}^{(i)})^2 + (\sum_i \sigma_{1e}^{(i)})^2 + (\sum_i \sigma_{ee}^{(i)})^2$ are denoted by $s(s+1)$, therefore, eigenvalues of $\sum_i \sigma_{ee}^{(i)}$ are $n_e/2 - s$. The eigenstates of H_1 can be classified according to N_e and s, and the eigenstates are described by $|s,n_e,n_c\rangle$. The states generated by the operators in H_1 from the eigenstates are described by

$$g\sigma_{e1}a|s,n_e,n_c\rangle = \sqrt{(s - n_e/2)(s + n_e/2 + 1)}\sqrt{n_c}g|s,n_e+1,n_c-1\rangle, \tag{B2}$$

$$g\sigma_{1e}a^\dagger|s,n_e,n_c\rangle = \sqrt{(s + n_e/2)(s - n_e/2 + 1)}\sqrt{n_c+1}g|s,n_e-1,n_c+1\rangle. \tag{B3}$$

The coefficients are called Clebsch-Gordan coefficients. In the operations by the operators, N_e is conserved. The eigenvalue of each case of N_e and s is described as follows.

1. The case of $N_e = 1$ and $s = N_2/2$

The ground state in the case of $N_e = 1$ and $s = N_2/2$ is $|N_2/2,0,1\rangle$, and the state which can be generated by H_1 is only $|N_2/2,1,0\rangle$. The matrix representation of H_1 is described by

$$H_1/\hbar = \begin{pmatrix} 0 & \sqrt{N_2}g \\ \sqrt{N_2}g & 0 \end{pmatrix}, \tag{B4}$$

with base of $(|N_2/2,0,1\rangle, |N_2/2,1,0\rangle)$. The eigenvalues which are obtained by diagonalization of the matrix are described by

$$E_n/\hbar = \pm\sqrt{N_2}g. \tag{B5}$$

In the case of $N = 3$, the eigenvalues are $E_n/\hbar = \pm\sqrt{2}g$ because of $N_2 = 2$.

2. The case of $N_e = 1$ and $s = N_2/2 - 1$

The ground state in the case of $N_e = 1$ and $s = N_2/2 - 1$ is $|N_2/2 - 1,1,0\rangle$. When the operators in H_1 [Eq. (B1)] operate the state, the state becomes zero vector. Therefore, the eigenvalue E_n is 0.

3. The case of $N_e = 2$ and $s = N_2/2$

The ground state in the case of $N_e = 2$ and $s = N_2/2$ is $|N_2/2,0,2\rangle$, and the states which can be generated by H_1 are $|N_2/2,1,1\rangle$ and $|N_2/2,2,0\rangle$. The matrix representation of H_1 is described by

$$H_1/\hbar = \begin{pmatrix} 0 & \sqrt{2N_2} & 0 \\ \sqrt{2N_2} & 0 & \sqrt{2(N_2-1)}g \\ 0 & \sqrt{2(N_2-1)}g & 0 \end{pmatrix}, \tag{B6}$$

with base of $(|N_2/2,0,2\rangle, |N_2/2,1,1\rangle, |N_2/2,2,0\rangle)$. The eigenvalues which are obtained by diagonalization of the matrix are described by

$$E_n/\hbar = 0, \pm\sqrt{4N_2 - 2}g. \tag{B7}$$

In the case of $N = 3$, the eigenvalues are $E_n/\hbar = 0, \pm\sqrt{10}g$ because of $N_2 = 3$.

4. The case of $N_e = 2$ and $s = N_2/2 - 1$

The ground state in the case of $N_e = 2$ and $s = N_2/2 - 1$ is $|N_2/2 - 1,1,1\rangle$, and the state which can be generated by

H_1 is only $|N_2/2-1,2,0\rangle$. The matrix representation of H_1 is described by

$$H_1/\hbar = \begin{pmatrix} 0 & \sqrt{N_2-2}g \\ \sqrt{N_2-2}g & 0 \end{pmatrix}, \tag{B8}$$

with base of $(|N_2/2-1,1,1\rangle, |N_2/2-1,2,0\rangle)$. The eigenvalues which are obtained by diagonalization of the matrix are described by

$$E_n/\hbar = \pm\sqrt{N_2-2}g. \tag{B9}$$

In the case of $N=3$, eigenvalues are $E_n/\hbar = \pm g$ because of $N_2 = 3$.

5. The case of $N_e = 2$ and $s = N_2/2-2$

The ground state in the case of $N_e = 2$ and $s = N_2/2-2$ is $|N_2/2-2,2,0\rangle$. When the operators in H_1 [Eq. (B1)] operate the state, the state becomes zero vector. Therefore, the eigenvalue E_n is 0.

The eigenvalues in the case of $N_e \geqslant 3$ can be derived by a similar calculation.

APPENDIX C: DERIVATION OF TABLE I

The regions represented by the equations in Table I are explained by the resonance conditions as follows. When the initial state is fixed to the state $|1210\rangle$, H can generate only the states of $(N_e,N_2) = (1,2),(2,3)$ in the states of $N_e \geqslant 1$. Therefore, the eigenvalues E_n contributing to the resonance conditions are only $\pm\sqrt{2}g$ ($N_e = 1$, $s = N_2/2 = 1$), 0, $\pm\sqrt{10}g$ ($N_e = 2$, $s = N_2/2 = 3/2$), and $\pm g$ ($N_e = 2$, $s = N_2/2-1 = 1/2$) in Eqs. (6). The resonance conditions obtained from $C_n^{(1)}$ [Eqs. (4)] using the above eigenvalues and $E_0 = 0$ are $\Delta = 0,g,\sqrt{2}g,\sqrt{10}g$, $\Delta_3 = 0,g,\sqrt{2}g,\sqrt{10}g$, and $\Delta+\Delta_3 = 0,g,\sqrt{2}g,\sqrt{10}g$ in the three-qubit system. In the case of $\Delta_3 \gg g$, the state of X_3 almost never transfers from a state $|1\rangle_3$, and the states of $N_2 = 3$ are almost never generated. Therefore, the error does not increase at $\Delta = g,\sqrt{10}g$ corresponding to the eigenvalues of $N_2 = 3$ in Fig. 2(a). The resonance conditions obtained from $C_n^{(2)}$ [Eqs. (5)] have a smaller contribution than the conditions obtained from $C_n^{(1)}$. However, when multiple conditions of Eqs. (5) are satisfied simultaneously, the contributions are not negligible. The conditions of such case are described by

$$\begin{aligned}(E_n-E_0)/\hbar = {} & 0,\pm\Delta,\pm\Delta_j,\pm2\Delta,\pm2\Delta_j,\pm(\Delta-\Delta_i),\\ & \pm(2\Delta+\Delta_j),\pm(\Delta+2\Delta_j),\pm2(\Delta+\Delta_j).\end{aligned} \tag{C1}$$

Some of the equations in Table I are explained by Eq. (C1). All of the 19 regions in which the errors increase in Fig. 2(c) are explained by analytic solution of second-order perturbation theory as above.

[1] M. A. Nielsen and I. L. Chuang, *Quantum Computation and Quantum Information*, 1st ed. (Cambridge University Press, Cambridge, 2000).
[2] P. Zanardi and M. Rasetti, Phys. Lett. A **264**, 94 (1999).
[3] L.-M. Duan, J. I. Cirac, and P. Zoller, Science **292**, 1695 (2001).
[4] Z. Kis and F. Renzoni, Phys. Rev. A **65**, 032318 (2002).
[5] K. Bergmann, H. Theuer, and B. W. Shore, Rev. Mod. Phys. **70**, 1003 (1998).
[6] B. Broers, H. B. van Linden van den Heuvell, and L. D. Noordam, Phys. Rev. Lett. **69**, 2062 (1992).
[7] L. S. Goldner, C. Gerz, R. J. C. Spreeuw, S. L. Rolston, C. I. Westbrook, W. D. Phillips, P. Marte, and P. Zoller, Phys. Rev. Lett. **72**, 997 (1994).
[8] H. Goto and K. Ichimura, Phys. Rev. A **74**, 053410 (2006).
[9] J. Klein, F. Beil, and T. Halfmann, Phys. Rev. Lett. **99**, 113003 (2007).
[10] J. Zhang, J. H. Shim, I. Niemeyer, T. Taniguchi, T. Teraji, H. Abe, S. Onoda, T. Yamamoto, T. Ohshima, J. Isoya, and D. Suter, Phys. Rev. Lett. **110**, 240501 (2013).
[11] K. Ichimura, Opt. Commun. **196**, 119 (2001).
[12] T. Pellizzari, S. A. Gardiner, J. I. Cirac, and P. Zoller, Phys. Rev. Lett. **75**, 3788 (1995).
[13] We take an expression of Rabi frequency without detuning. In general, $|1\rangle_j - |e\rangle_j$ transitions of X_i have different Rabi frequencies of L_1 because the transitions have different dipole moments and positions of X_i are different from each other with respect to the cavity mode. However, we assume that the Rabi frequencies are a common Ω_1 for simplicity.
[14] H. Goto and K. Ichimura, Phys. Rev. A **77**, 013816 (2008).
[15] G. S. Agarwal, Phys. Rev. Lett. **53**, 1732 (1984).
[16] G. Varada, M. Kumar, and G. Agarwal, Opt. Commun. **62**, 328 (1987).
[17] M. B. Plenio and P. L. Knight, Rev. Mod. Phys. **70**, 101 (1998).
[18] R. Kolesov, K. Xia, R. Reuter, R. Stöhr, A. Zappe, J. Meijer, P. Hemmer, and J. Wrachtrup, Nat. Commun. **3**, 1029 (2012).
[19] Y. Yan, J. Karlsson, L. Rippe, A. Walther, D. Serrano, D. Lindgren, M.-e. Pistol, S. Kröll, P. Goldner, L. Zheng, and J. Xu, Phys. Rev. B **87**, 184205 (2013).
[20] M. P. Hedges, J. J. Longdell, Y. Li, and M. J. Sellars, Nature (London) **465**, 1052 (2010).
[21] N. Sangouard, C. Simon, H. de Riedmatten, and N. Gisin, Rev. Mod. Phys. **83**, 33 (2011).
[22] K. Holliday, M. Croci, E. Vauthey, and U. P. Wild, Phys. Rev. B **47**, 14741 (1993).
[23] H. Goto, S. Nakamura, and K. Ichimura, Opt. Express **18**, 23763 (2010).
[24] K. Ichimura and H. Goto, Phys. Rev. A **74**, 033818 (2006).
[25] R. W. Equall, R. L. Cone, and R. M. Macfarlane, Phys. Rev. B **52**, 3963 (1995).
[26] The cavity-relaxation rate κ is described by $\kappa/2\pi = c(L+T_1+T_2)/8\pi nd$, where L is the loss of cavity per round trip, $T_{1,2}$ are the transmittances of mirrors, n is the refractive index of the crystal, d is a cavity length, and c is the speed of light [23]. A sample of Ref. [23] has $\kappa/2\pi \sim 1.3$ MHz, $L \sim 10^{-3}$, $T_{1,2} = 0.3\times10^{-3}$, $d \sim 7.5$ mm, and $n \sim 1.9$. Because $T_{1,2}$ will be reduced smaller than 10^{-6}, κ will be reduced as L decreases. When L is reduced

to 10^{-6}, $\kappa/2\pi$ will be reduced to 1 kHz. The loss of 10^{-6} is the same or a larger level as the ultralow-loss mirrors [32] and some low-loss materials such as optical fiber.

[27] The coupling constant g is proportional to the mode waist of the cavity. A sample of Ref. [24] has $g/2\pi \sim 15$ kHz and the mode waist of 50 μm. If the mode waist becomes wavelength scale, then $g/2\pi$ will increase to 1 MHz.

[28] T. Gaebel, M. Domhan, I. Popa, C. Wittmann, P. Neumann, F. Jelezko, J. R. Rabeau, N. Stavrias, A. D. Greentree, S. Prawer, J. Meijer, J. Twamley, P. R. Hemmer, and J. Wrachtrup, Nat. Phys. **2**, 408 (2006).

[29] P. E. Barclay, K. M. Fu, C. Santori, and R. G. Beausoleil, Opt. Express **17**, 9588 (2009).

[30] P. E. Hemmer, A. V. Turukhin, M. S. Shahriar, and J. A. Musser, Opt. Lett. **26**, 361 (2001).

[31] G. Balasubramanian, I. Y. Chan, R. Kolesov, M. Al-Hmoud, J. Tisler, C. Shin, C. Kim, A. Wojcik, P. R. Hemmer, A. Krueger, T. Hanke, A. Leitenstorfer, R. Bratschitsch, F. Jelezko, and J. Wrachtrup, Nature (London) **455**, 648 (2008).

[32] G. Rempe, R. Lalezari, R. J. Thompson, and H. J. Kimble, Opt. Lett. **17**, 363 (1992).